Soft Matter

PAPER

View Article Online
View Journal | View Issue

Cite this: *Soft Matter*, 2019, **15**, 1260

Influence of polymer flexibility on nanoparticle dynamics in semidilute solutions†

Renjie Chen,[a] Ryan Poling-Skutvik,[a] Michael P. Howard,[b] Arash Nikoubashman,[c] Sergei A. Egorov,[de] Jacinta C. Conrad[a] and Jeremy C. Palmer*[a]

Received 8th September 2018,
Accepted 7th November 2018

DOI: 10.1039/c8sm01834k

rsc.li/soft-matter-journal

The hierarchical structure and dynamics of polymer solutions control the transport of nanoparticles (NPs) through them. Here, we perform multi-particle collision dynamics simulations of solutions of semiflexible polymer chains with tunable persistence length l_p to investigate the effect of chain stiffness on NP transport. The NPs exhibit two distinct dynamical regimes – subdiffusion on short time scales and diffusion on long time scales. The long-time NP diffusivities are compared with predictions from the Stokes–Einstein relation (SER), mode-coupling theory (MCT), and a recent polymer coupling theory (PCT). Increasing deviations from the SER as the polymer chains become more rigid (*i.e.* as l_p increases) indicate that the NP motions become decoupled from the bulk viscosity of the polymer solution. Likewise, polymer stiffness leads to deviations from PCT, which was developed for fully flexible chains. Independent of l_p, however, the long-time diffusion behavior is well-described by MCT, particularly at high polymer concentration. We also observed that the short-time subdiffusive dynamics are strongly dependent on polymer flexibility. As l_p is increased, the NP dynamics become more subdiffusive and decouple from the dynamics of the polymer chain center-of-mass. We posit that these effects are due to differences in the segmental mobility of the semiflexible chains.

1 Introduction

Transport of nanoparticles (NPs) through complex heterogeneous fluids underlies the efficacy of targeted drug delivery methods,[1–3] the ability of NPs to modify rheological or surface tension properties of fluids,[4–7] and the functionalization of nanocomposites.[8,9] Traditionally, the Brownian motion of spherical particles is described by the Stokes–Einstein relation (SER), in which the mobility is inversely related to the viscous drag, *via* $D = k_B T/(z\pi\eta_0\sigma_{NP})$, where D is the particle diffusivity, k_B is Boltzmann's constant, T is the temperature, η_0 is the zero-shear viscosity of the solution, σ_{NP} is the NP diameter, and $z = 2$ or 3 for slip or no-slip boundary conditions at the particle surface, respectively. This relationship can be extended for complex fluids by incorporating a complex (frequency-dependent) solution viscosity $\tilde{\eta}$ according to the generalized Stokes–Einstein relation (GSER).[10,11] Both the SER and GSER assume that the suspended particle is large enough that any heterogeneity of the fluid is negligible over the particle surface. This assumption is broken, however, if the particle size is comparable to or smaller than characteristic length scales of the medium, which is commonly encountered for NPs suspended in polymer solutions or melts. In this limit, dynamics deviate from the prediction of the GSER,[12–19] confirming that complex viscosity $\tilde{\eta}$ alone is insufficient to predict the motion of particles in heterogeneous polymer solutions.

To describe the diffusion of NPs through polymer meshes, early theoretical arguments used obstruction,[20,21] hydrodynamic,[22–24] and free volume[25] approaches. More recently, mode-coupling theory (MCT)[26,27] and self-consistent Langevin equations[28] have been used to relate the fluctuations in the polymer mesh to the NP dynamics. These methods provide predictions of the NP long-time diffusivity, but do not access their short time dynamics. A recent polymer coupling theory (PCT),[29] based on scaling arguments for polymer dynamics,[30,31] assumes that the NP dynamics fully couple to segmental relaxations of the polymers on comparable length scales. This model, which predicts that the dynamics are controlled by the ratio of σ_{NP} to the polymer correlation length ξ, correctly captures the change in long-time diffusivity as the particle size or polymer

[a] *Department of Chemical and Biomolecular Engineering, University of Houston, Houston, TX 77204, USA. E-mail: jcpalmer@uh.edu*
[b] *McKetta Department of Chemical Engineering, University of Texas at Austin, Austin, TX 78712, USA*
[c] *Institute of Physics, Johannes Gutenberg University Mainz, Staudingerweg 7, 55128 Mainz, Germany*
[d] *Department of Chemistry, University of Virginia, Charlottesville, Virginia 22901, USA*
[e] *Leibniz Inst Polymer Res Dresden, Hohe Strasse 6, D-01069 Dresden, Germany*

† Electronic supplementary information (ESI) available: Discussion of methods for calculating zero-shear viscosity and associated data. See DOI: 10.1039/c8sm01834k

concentration is changed.[18] On short length and time scales, however, experiments and simulations suggest that the particle dynamics are incompletely coupled to the segmental dynamics of flexible polymers and additionally couple to the center-of-mass relaxations of the polymers.[18,32–34]

For semiflexible polymers, theoretical descriptions based on simple scaling laws are expected to be even less fruitful because stiff macromolecules cannot be described by a self-similar fractal structure. Instead, semiflexible chains are characterized by several crossover length scales, such as the persistence and contour lengths, which introduce a large number of disparate time and length scales that are relevant to describing their dynamics. Accordingly, it has been shown that even modest stiffness affects both static[35–38] and dynamic[39–41] properties of polymer liquids. This scenario is relevant for understanding transport through the intracellular space, crowded by actin, microtubules, and other semiflexible biopolymers.[42,43] On short time scales the motion of microscale particles (larger than the mesh size or correlation length) is subdiffusive, scaling with time with an exponent of 3/4[44,45] as predicted from the microscopic relaxations of semiflexible polymers.[46,47] Surprisingly, how smaller particles couple to the dynamics of semiflexible chains has not been systematically explored and is the focus of this study.

In this work, we use a combination of simulation and theory to probe NP dynamics in solutions of semiflexible polymers, whose stiffnesses are characterized by the persistence length l_p. The colloidal suspensions are simulated using a hybrid molecular dynamics–multi-particle collision dynamics (MD–MPCD) scheme, which accounts for hydrodynamic interactions through the use of an explicit coarse-grained solvent. The simulation results are also compared with predictions from MCT[26] for concentrated polymer solutions. The NP dynamics are subdiffusive on short time scales and diffusive on long time scales. The long-time diffusivities scale with the polymer correlation length at low polymer concentrations in agreement with PCT, but depend on polymer stiffness at higher concentrations. Good agreement is also observed with the long-time diffusivities calculated from MCT at high polymer concentrations, where the theory is expected to be most accurate. The short-time subdiffusive dynamics, by contrast, vary strikingly with the flexibility of the polymers. For fully flexible polymers whose characteristic length scales are comparable to the NP size, we observe that the subdiffusive behavior of the NPs is coupled to the polymer center-of-mass motion, in accord with our previous study.[34] As l_p is increased such that the polymer chains become more rigid, however, the dynamics of the NPs become more subdiffusive and decouple from the dynamics of the polymer chain center-of-mass. These effects likely arise from changes in the segmental relaxations as the chain stiffness is increased.

2 Methods

Molecular dynamics simulations of the NP–polymer systems were performed with LAMMPS.[48] For convenience in describing the model system, we define σ, m, and ε as the fundamental base units for length, mass, and energy, respectively. The corresponding unit of time is $\tau = \sqrt{m\sigma^2/\varepsilon}$. All physical quantities are reduced using these fundamental base units and reported in dimensionless form.

We adopted similar models to those used in our previous study of NP dynamics in solutions of fully flexible polymer chains.[34] Nanoparticles were modeled as large spheres with diameter $\sigma_{NP} = 5$. Polymers were represented by the Kremer–Grest (KG) model[49] as linear chains composed of $N_m = 32$ smaller beads with diameter $\sigma_P = 1$. Excluded volume interactions were modeled using the shifted Weeks–Chandler–Andersen (sWCA) potential[50]

$$U_{\mathrm{sWCA}}(r_{ij}) = \begin{cases} 4\varepsilon_{ij}\left[\left(\frac{\sigma_{ij}}{r_{ij}-\Delta_{ij}}\right)^{12} - \left(\frac{\sigma_{ij}}{r_{ij}-\Delta_{ij}}\right)^{6}\right] + \varepsilon_{ij}, & r_{ij} \le r_{ij}^{c} \\ 0, & r_{ij} > r_{ij}^{c} \end{cases}, \quad (1)$$

where r_{ij} is the scalar separation distance between particles i and j, $\varepsilon_{ij} = 1$ is the parameter controlling the strength of the repulsion, and the potential is truncated and shifted at $r_{ij}^{c} = 2^{1/6}\sigma_{ij} + \Delta_{ij}$. For NP–NP and monomer–monomer interactions we used $\sigma_{ij} = \sigma_{NP}$ and $\sigma_{ij} = \sigma_P$, respectively, and set $\Delta_{ij} = 0$. For NP–monomer interactions, we chose $\sigma_{ij} = \sigma_P$ and $\Delta_{ij} = (\sigma_{NP} - \sigma_P)/2$ to account for their size asymmetry.

Adjacent beads on each polymer chain were connected by anharmonic springs described using the finitely extensible nonlinear elastic (FENE) potential,[51]

$$U_{\mathrm{FENE}}(r_{ij}) = \begin{cases} -\frac{1}{2}kr_0^2 \ln\left[1 - \frac{r_{ij}^2}{r_0^2}\right], & r_{ij} \le r_0 \\ \infty, & r_{ij} > r_0 \end{cases}, \quad (2)$$

with spring constant $k = 30$ and maximum bond extension $r_0 = 1.5$. Chain stiffness was incorporated into the KG model using the bending potential[40,41,52–54]

$$U_{\mathrm{bend}}(\Theta_{ijk}) = \kappa(1 - \cos\Theta_{ijk}) \quad (3)$$

where Θ_{ijk} is the angle between the bonds connecting consecutive beads i to j and j to k (an angle of $\Theta_{ijk} = 0^\circ$ corresponds to three beads in a line). The parameter κ modulates the strength of the potential and stiffness of the chains. For sufficiently stiff polymers ($\kappa > 2$), it is related to the chain persistence length *via* $l_p \approx b\kappa$,[40] where b is the equilibrium bond length ($b \approx 0.97$ for the standard parameterization of the KG model). The contour length of the chain is given by $L_c = (N_m - 1)b \approx 30$.

To study the influence of chain flexibility on NP dynamics, we performed simulations using different values of κ ranging from 0 (fully flexible) to 32 ($l_p/L_c \approx 1$) (Table 1 and Fig. 1). The edge length of the box ($L = 64$) was chosen to be approximately eight times the radius of gyration $R_{g,0}$ of the stiffest polymer ($\kappa = 32$) at infinite dilution to minimize finite-size effects. All simulations were conducted in a cubic box with periodic boundary conditions in each direction. For highly flexible polymers ($\kappa \le 2$), the number of polymer chains N_c was varied

Table 1 Properties of the polymer systems investigated in this study

κ	l_p/L_c	$R_{g,0}$	ν	c_{min}	c_{max}
0	0.03	3.63	0.61	0.025 (0.16 c^*)	0.50 (3.13 c^*)
2	0.06	4.37	0.62	0.025 (0.27 c^*)	0.40 (4.37 c^*)
5	0.15	5.62	0.62	0.025 (0.58 c^*)	0.40 (9.29 c^*)
10	0.31	6.82	0.66	0.025 (1.04 c^*)	0.40 (16.61 c^*)
20	0.63	7.73	0.74	0.025 (1.51 c^*)	0.25 (15.12 c^*)
32	1.01	8.15	0.81	0.025 (1.77 c^*)	0.25 (17.72 c^*)

Notes: c_{min} and c_{max} are the minimum and maximum monomer concentrations investigated in this study, and $c^* = 3N_m(4\pi R_{g,0}^3)^{-1}$ is the overlap concentration.

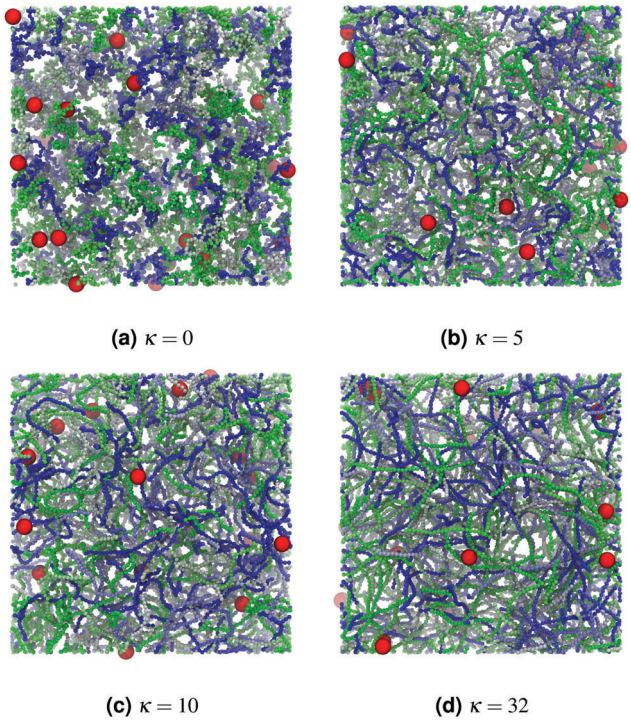

Fig. 1 Nanoparticles (red) in solutions of (a) fully flexible, (b and c) semiflexible, and (d) stiff polymer chains with monomer concentration $c = 0.05$. Polymers simulated using a given κ are identical, but have been colored by chain index to enhance visual clarity. Snapshots rendered using Visual Molecular Dynamics 1.9.3.[55]

from 200 to 4900, to achieve monomer concentrations $c = N_c N_m L^{-3}$ ranging from 0.025 to 0.5. At higher values of κ, however, the maximum value of c was further limited to avoid the well-characterized isotropic–nematic transition in this system[37] and stay within the isotropic phase (Table 1). The number of NPs was fixed at 20 in each simulation (volume fraction $\approx$ 0.005) to improve sampling while keeping NP–NP interactions negligible.

Molecular dynamics trajectories were propagated using a velocity-Verlet integrator with time step 0.005. Simulations for $\kappa \leq 10$ were equilibrated for at least $10^5\tau$, whereas longer periods of $\approx 10^6\tau$ were used for $\kappa \geq 20$ to account for slower relaxation of these systems. Equilibration was followed by a production period of $\approx 10^6\tau$ during which trajectories were saved for subsequent analysis. Ensemble averages were computed from three independent simulations (60 NP trajectories), and statistical uncertainties were estimated from the standard error. Hydrodynamic interactions (HI) were incorporated by coupling the MD particles to a coarse-grained solvent modeled using the multi-particle collisions dynamics (MPCD) method.[56–59] Implementation details of the hybrid MD–MPCD algorithm are identical to those reported in our previous study.[34] Briefly, the MD–MPCD simulations were performed using a collision cell edge length $a = 1$, a solvent particle mass $m_s = 1$, an average solvent density $\rho = 5$ (5 solvent particles per collision cell), and a collision time step 0.09. Solvent collisions were handled using a momentum-conserving version of the Andersen thermostat[60,61] with a set temperature $T = 1$. Further, the reference positions of the cells were randomly shifted before each collision step to ensure Galilean invariance.[62] These choices give an MPCD solvent with Schmidt number Sc $\approx$ 12.0 and dynamic viscosity $\eta_s \approx 4.0$. Solvent–polymer collisions were handled using the scheme discussed in ref. 63, whereas momentum transfer between the solvent and NPs was treated using the stochastic boundary algorithm described in ref. 64 with slip conditions. To achieve neutral buoyancy in the background solvent, the masses of the polymer beads and NPs were set to $m_P = \rho\sigma_P^3$ and $m_{NP} = \rho\pi\sigma_{NP}^3/6$, respectively.

To compare the simulated NP diffusivities to the SER, the shear viscosities of the polymer solutions were determined through reverse nonequilibrium molecular dynamics (RNEMD) simulations[41,65] using HOOMD-blue with MD[66–68] and MPCD[69] accelerated on graphics processing units. Stress was imposed on the solutions by generating a momentum flux, and the shear rate was extracted from the emerging flow profile. For the fully flexible chains we were able to directly access the linear response regime and measure the zero-shear viscosity η_0. As the stiffness was increased, however, the polymer relaxation slowed down significantly, making a direct measurement of η_0 computationally infeasible. In these cases, we extracted the zero-shear viscosity by fitting our data to the Cross model (ESI).[41,70,71] Uncertainties in η_0 from this fitting procedure were estimated and propagated using standard relationships to calculate errors in other quantities derived from these values.

3 Results and discussion

We first characterized the structure of the polymer chains as the stiffness κ was varied. Polymer chains are fractal, and their radius of gyration in dilute solution $R_{g,0}$ scales with the number of monomer beads N_m as $R_{g,0} \sim N_m^{\nu}$, where ν is the excluded volume exponent. For fully flexible chains (*i.e.* $\kappa = 0$), we found $\nu \approx 0.61$ (Fig. 2 and Table 1), which is in good agreement with theoretical predictions and previous simulation results of self-avoiding chains in a good solvent.[34,72] As the chain stiffness increased, the polymer chains became more rod-like, which is reflected by the increasing excluded volume exponent ν. However, ν remained below the physical limit for hard rods ($\nu = 1$) and reached a value of $\nu \approx 0.81$ for the largest investigated stiffness of $\kappa = 32$ (Fig. 2 and Table 1).

After confirming that the simulated polymer structure agrees with theoretical predictions, we analyzed the dynamics

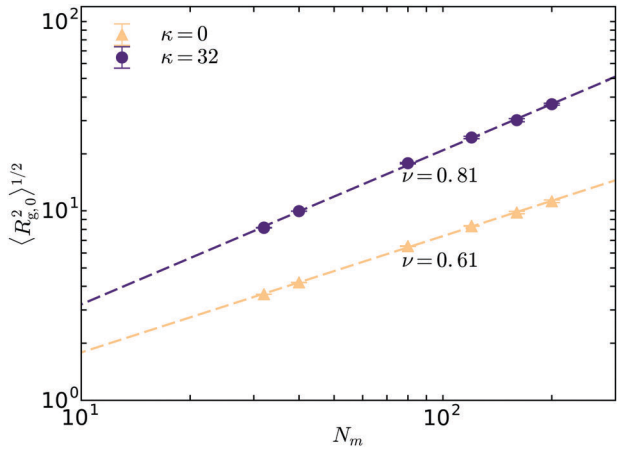

Fig. 2 Scaling of radius of gyration $R_{g,0}$ in dilute solution as a function of the number of monomer beads N_m for polymers with stiffness κ = 0 (△) and 32 (○). Dashed lines are power law fits.

of the constituents of the suspensions. From the MPCD simulations, we calculated the mean-squared displacement $\langle \Delta r^2 \rangle$ for the monomers in the reference frame of the polymer centers-of-mass (COM), for the polymer COM, and for the dispersed NPs as functions of chain stiffness κ (Fig. 3). For fully flexible chains (*i.e.* κ = 0), monomers are hydrodynamically coupled and move according to Zimm dynamics on short time scales with $\langle \Delta r^2 \rangle \sim t^{2/3}$, as expected.[72] As κ increases, the monomers remain hydrodynamically coupled, but the chains become stiffer and their segmental mobility decreases (Fig. 3(a)).

The chain stiffness also affects the motion of the polymer COM (Fig. 3(b)). On short time scales, the mean-squared displacement of the polymer COM develops a subdiffusive region as κ increases, in which $\langle \Delta r^2 \rangle \sim t^{\alpha}$ and $\alpha < 1$ is the subdiffusive exponent. On long time scales, the MSD of the polymer COM recovers diffusive scaling $\alpha = 1$ with the diffusivity decreasing with κ due to lower segmental mobility and larger size of the stiffer chains. The motion of the NPs (Fig. 3(c)) is qualitatively similar to that of the polymer COM with a pronounced subdiffusive region when dispersed in solutions of stiff chains.

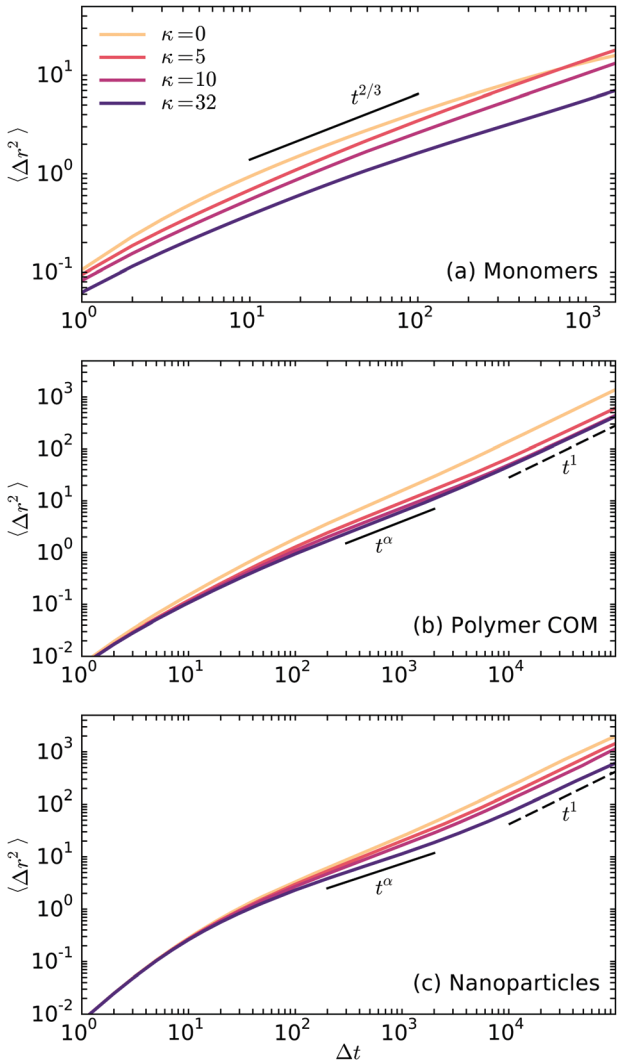

Fig. 3 Mean-squared displacement $\langle \Delta r^2 \rangle$ as a function of lag time Δt at multiple polymer stiffnesses and monomer concentration c = 0.20 for (a) the monomers in the reference frame of the polymer centers-of-mass (COM), (b) the polymer COM, and (c) the NPs. Dashed and solid lines indicate diffusive ($\sim t^1$) and subdiffusive ($\sim t^{\alpha}$, $\alpha < 1$) scaling, respectively.

3.1 Long-time nanoparticle diffusivity

The effect of polymer stiffness on the dynamics of NPs was further characterized by calculating their long-time diffusivity D and short-time subdiffusive exponent α_{NP}. To facilitate quantitative comparisons with theory, the NP diffusivities measured in the simulations, $D(L)$, were corrected for finite-size effects using[73]

$$D = \left(1 - \frac{\zeta \sigma_{NP}}{3L}\right)^{-1} \times D(L) \approx 1.08 \times D(L) \qquad (4)$$

where ζ = 2.837297. Eqn (4) corrects for finite-size effects associated with long-range hydrodynamic interactions between periodic images of the simulation box, which vanish as $L \to \infty$ and are thus not present in infinite systems. This expression is valid for NPs with a slip boundary condition at their surface, but analogous expressions have also been derived for no-slip boundary conditions.[73] For the system considered here (L = 64, σ_{NP} = 5), the correction is relatively small and increases the diffusivity by ≈8%.

The values of D from simulation are significantly larger than the diffusivities predicted by the SER (Fig. 4), indicating that the motions of the NPs are incompletely coupled to the bulk viscosity of the background polymer solutions. Deviations from SER predictions have also been observed in experimental studies performed on NPs in solutions of similarly sized polymers,[16,18] ranging from $D/D_{SER} \approx 2$ when $\sigma_{NP}/2R_{g,0} \approx 0.9$ to $D/D_{SER} \approx 30$ when $\sigma_{NP}/2R_{g,0} \approx 0.6$. They arise because the NPs are comparably sized to the polymer chains, which violates the homogeneity assumption underlying the SER.[14] The deviations from SER predictions become more pronounced as the chains become stiffer, indicating that the NPs become increasingly decoupled from the bulk solution viscosity. For simulations of

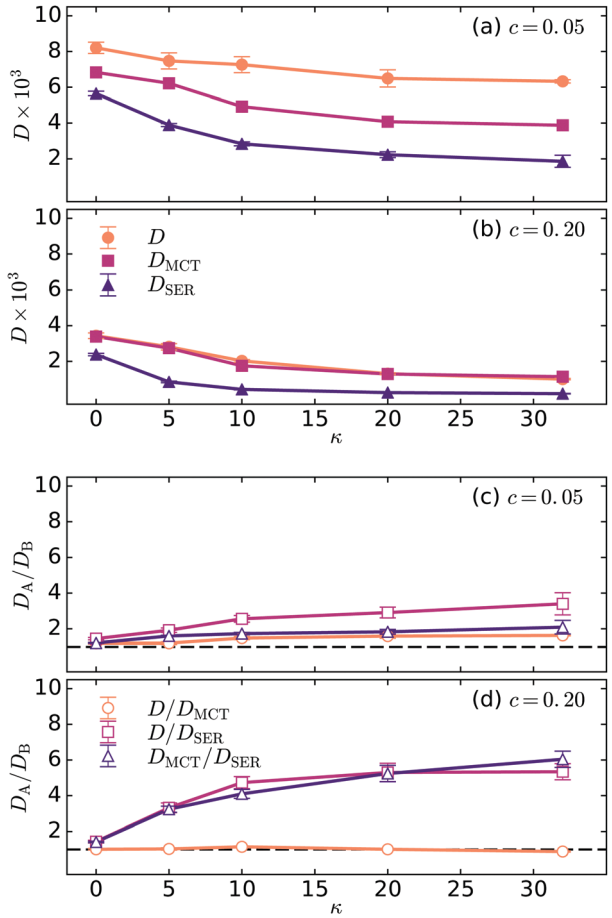

Fig. 4 NP diffusivity obtained from MD–MPCD simulations with finite size correction following ref. 73 (D), from MCT calculations (D_{MCT}), and from the SER (D_{SER}). Closed symbols in (a) and (b) indicate diffusivities and open symbols in (c) and (d) indicate ratios of diffusivities. Dashed lines in (c) and (d) indicate a diffusivity ratio of unity.

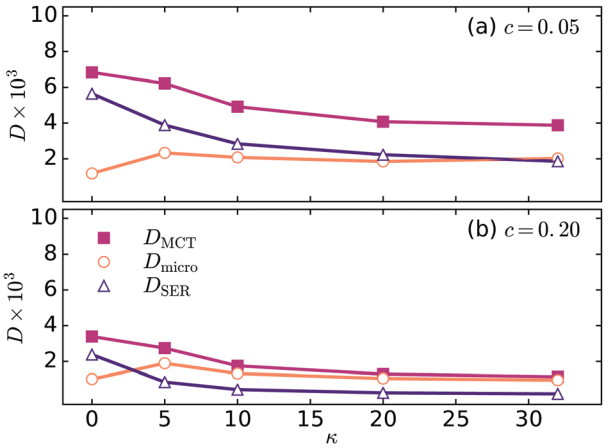

Fig. 5 NP diffusivity obtained from the MCT calculations broken down into hydrodynamic (D_{SER}) and non-hydrodynamic (D_{micro}) contributions for polymer concentrations (a) c = 0.05 and (b) c = 0.20.

NPs in solutions of infinitely rigid rods, these deviations were posited to develop because of constraint release mechanisms in the rod matrix.[74]

We also compared our simulation results to calculations performed using a variant of MCT developed for dense polymer solutions.[26,27] Details of the MCT calculations follow those in ref. 26 and are thus not repeated here. Within MCT, the overall NP diffusion coefficient D_{MCT} is written as a sum of hydrodynamic and non-hydrodynamic (microscopic) terms.[26,27] The former is given by D_{SER}, whereas the latter contribution, D_{micro}, arises due to the coupling of the NP motion to polymer collective density modes.[26,27] Calculation of D_{micro} requires several structural (NP–monomer and monomer–monomer radial distribution functions and $R_{g,0}$) and dynamical (monomer diffusion coefficient) quantities as input.[26] These quantities can be calculated directly from theory,[26] but here we use input from the MD–MPCD simulation, as our main interest is to test the approximations inherent in MCT. In computing D_{micro}, we also include the contribution arising from the coupling to the self-transverse current mode given in ref. 75, which affects the dynamic shear viscosity and has been shown to play an important role in treating diffusion in low-density fluids.[75] Although this additional contribution is negligible in dense systems, we nonetheless include it in all MCT calculations and evaluate it using input from the MD–MPCD simulation.

The relative contributions of D_{SER} and D_{micro} to D_{MCT} depend on polymer concentration for the small particles examined here; D_{SER} is comparable to D_{micro} at low polymer concentrations (c = 0.05, Fig. 5(a)) but much smaller than D_{micro} at high polymer concentrations (c = 0.20, Fig. 5(b)), as also seen in an earlier MCT study.[26] The overall diffusivities D_{MCT} predicted by MCT are in excellent agreement with those calculated from the MD–MPCD simulations (Fig. 4) at polymer concentration c = 0.20 for all values of κ examined.

For lower concentration c = 0.05, however, deviations between MCT and simulation are observed. Even with incorporation of the contribution from the coupling to the self-transverse current mode, MCT systematically underestimates the NP diffusivity at c = 0.05. This discrepancy is presumably due to the fact that additional collective modes, which have not been taken into account, are important at these conditions. Nevertheless, the overall agreement with simulation is reasonable, and MCT correctly captures the increasingly significant deviations from SER as the polymers become stiffer.

Lastly, we compared the behavior of the NP diffusivity with predictions from the PCT developed in ref. 29 for fully flexible polymers to explain deviations from the SER. This theory assumes that the NPs are locally caged by polymers until the surrounding chains relax over the particle surface. Accordingly, the long-time NP diffusivity is predicted to depend on the length-scale ratio of NP diameter to polymer correlation length σ_{NP}/ξ and to scale as $D/D_0 \sim (\sigma_{NP}/\xi)^{-2}$, where D_0 is the nanoparticle diffusivity in pure solvent. For $c/c^* > 1$ we used $\xi = R_{g,0}(c/c^*)^{-\nu/(3\nu-1)}$ from scaling theory,[72] where $c^* = 3N_m(4\pi R_{g,0}{}^3)^{-1}$ is the overlap concentration (Table 1). For $c/c^* \leq 1$, we calculated ξ according to the mean geometric separation distance $R_{g,0}(c/c^*)^{-1/3}$. We verified this PCT prediction experimentally[18] and with simulations[34] in previous work for fully

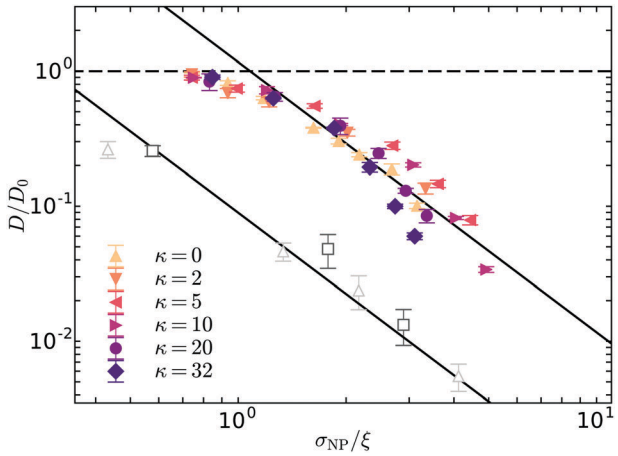

Fig. 6 Normalized NP diffusivity D/D_0 as a function of size ratio σ_{NP}/ξ for polymers with varying stiffness κ. Open symbols are experimental data from ref. 18 with $\sigma_{NP}/2R_{g,0}$ = 0.56 (△), 0.74 (□). Solid lines are scaling predictions[29] $D/D_0 \sim (\sigma_{NP}/\xi)^{-2}$.

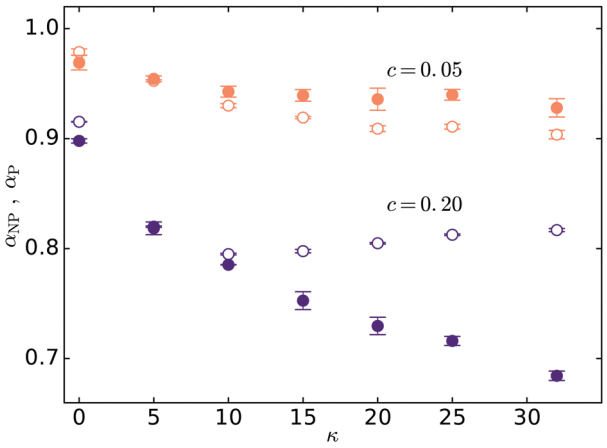

Fig. 7 Subdiffusive exponent of NPs α_{NP} (closed) and polymer centers-of-mass α_P (open) as a function of bending constant κ, for monomer concentrations of c = 0.05 (orange) and c = 0.20 (purple).

flexible chains in solution. By contrast, tests of PCT in computational studies of nanoparticle–polymer composites modeled using flexible chains have yielded inconclusive results.[76] Here, we extend tests of this scaling relation to semiflexible polymer solutions (Fig. 6).

At very low polymer concentrations, the NP diffusivities remain mostly unaffected by the polymers so that $D/D_0 \approx 1$. The diffusivities decrease with increasing polymer concentration solely as a function of length-scale ratio σ_{NP}/ξ. In solutions of flexible chains ($\kappa \approx 0$), the NP diffusivities eventually cross over and scale according to $D/D_0 \sim (\sigma_{NP}/\xi)^{-2}$ at large σ_{NP}/ξ, in agreement with the PCT predictions of ref. 29. Similar behavior for flexible chains was also observed in our previous study,[34] where the agreement with PCT was even more clear due to the use of longer polymer chains (N_m = 50), which provided access to larger σ_{NP}/ξ.[34] Slightly shorter chains (N_m = 32) were used in this study to avoid approaching the isotropic–nematic transition in systems with stiff chains.[37] Agreement with PCT was also observed experimentally for flexible chains,[18] although vertically offset from the simulation results due to differences in solution viscosity.[34] For stiffer chains (large κ), however, the NP diffusivities decrease more rapidly and deviate from the predicted scaling. According to PCT, the long-time dynamics depend on the segmental relaxations of the polymer chains. Thus, the different diffusivity dependences likely arise from the slower monomer dynamics of the stiffer chains (Fig. 3(a)). As the monomer dynamics slow down with increasing κ, the time required for the polymer mesh to relax over the particle surface increases. This longer relaxation thereby slows the long-time NP motion.

3.2 Short-time subdiffusion

Beyond segmental mobility, the dynamics of the polymer COM also play an important role in controlling the subdiffusive motion of dispersed NPs.[34] For flexible chains, both Rouse and Zimm theories assume that the COM of polymer chains move diffusively on all time scales.[72] Experimentally, however, the COM dynamics of polymers deviate from this diffusive assumption and move subdiffusively on short time scales.[77] Our simulations reveal that the subdiffusive dynamics of the polymer COM depend on both polymer concentration and chain stiffness (Fig. 7). For both concentrations, the subdiffusive exponent α_P for the polymer COM initially decays with increasing κ before reaching a plateau. Higher polymer concentrations lead to lower values of α_P for all κ. The NP subdiffusive exponent α_{NP} also decreases as the polymer concentration and κ are increased, similar to α_P. It does not, however, reach a plateau at high κ for the higher polymer concentration (c = 0.20), unlike α_P.

When particles are much larger than characteristic length scales in the polymer, ($\sigma_{NP} \gg 2R_{g,0}$), their short-time dynamics directly follow the segmental relaxations of the free polymer. This coupling results in subdiffusive particle dynamics in the microrheological limit, with α_{NP} = 0.5 in solutions of flexible polymer[18,29,78] and α_{NP} = 3/4 in solutions of semiflexible chains.[44,45] The PCT developed for smaller (nano)particles in ref. 29 still assumes direct coupling of the NP to segmental relaxations of the surrounding polymer chains on short time scales, so that α_{NP} exhibits a step change and abruptly decreases from 1 to 0.5 at σ_{NP}/ξ = 1 (Fig. 8). For flexible chains, such a step change is not observed in experiments[18] or simulations.[34] Instead, α_{NP} smoothly decreases as the size ratio σ_{NP}/ξ increases. For stiff chains, the shape of this decay changes (Fig. 8). At low polymer concentrations, α_{NP} decreases with increasing polymer concentration independent of κ. At higher polymer concentrations (*i.e.* larger σ_{NP}/ξ), the NP dynamics become increasingly subdiffusive with increasing polymer stiffness. The steeper decays suggest that the NP dynamics couple differently to the segmental mobility of stiffer chains.

In previous work,[34] we attributed the deviation from scaling predictions on short time scales to the coupling of the NP dynamics to both the segmental relaxations of the polymer chains and to the dynamics of the polymer COM. To assess the degree to which NP dynamics couple to segmental relaxations and the dynamics of polymer COM in solutions of semiflexible chains,

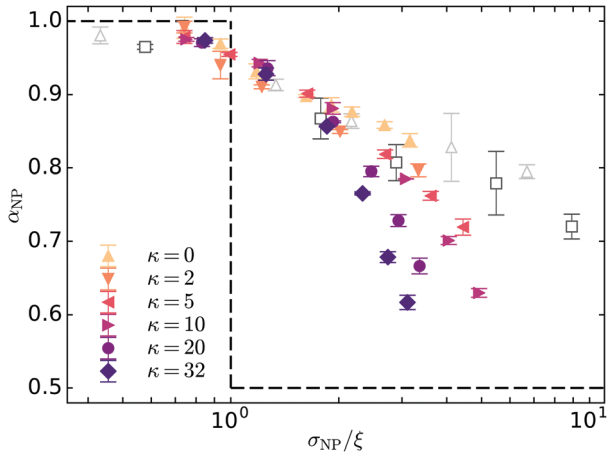

Fig. 8 Subdiffusive exponent of NP α_{NP} as a function of particle diameter σ_{NP} to polymer correlation length ξ size ratio for chains with varying stiffness κ. Open symbols are experimental data from ref. 18 with $\sigma_{NP}/2R_{g,0}$ = 0.56 (△), 0.74 (□). Dashed lines are predictions from PCT in solutions of flexible polymer chains.[29]

we analyze the correlation between α_{NP} and α_P (Fig. 9). At low polymer concentrations, the dynamics of the NPs and polymer COM are largely diffusive for all κ with $\alpha_{NP} = \alpha_P \approx 1$. As the polymer concentration increases, α_{NP} decreases concomitant with α_P for all κ, indicating that the NP and polymer COM dynamics are correlated in these solutions. At higher polymer concentrations, however, α_{NP} decouples from α_P and decreases more rapidly with increasing chain stiffness. The stronger subdiffusion of NPs in solutions of stiff chains is a marked difference from the predicted microrheological behavior of micron-sized particles in solutions of semiflexible chains in which $\alpha_{NP} = 3/4$.[44,45] The decorrelation of the short-time dynamics of nanoparticles and polymer COM suggests that the NPs couple more strongly to the decreased monomer dynamics of the surrounding chains in solutions of semiflexible chains. This hypothesis is consistent with the steeper decay of α_{NP} with polymer concentration (Fig. 8).

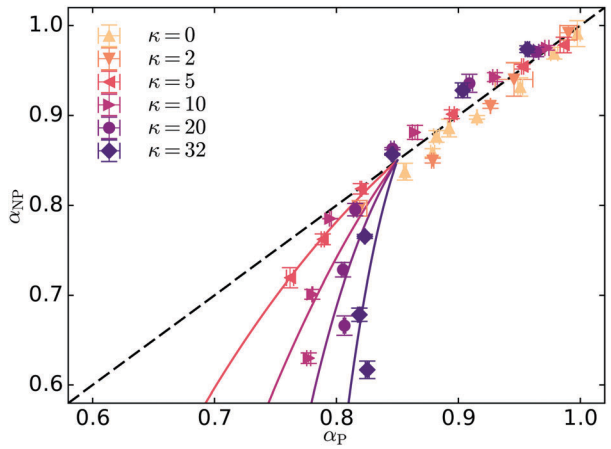

Fig. 9 Correlations between subdiffusive exponent of NPs α_{NP} and polymer centers-of-mass α_P for polymers with varying stiffness κ. Dashed line indicates $\alpha_{NP} = \alpha_P$, and solid lines are guides to the eye.

4 Conclusions

Understanding the effects of polymer stiffness on NP transport is critical to improving the efficacy of composite processing and drug delivery. Here, we performed hybrid MD–MPCD simulations of semidilute solutions of polymers with tunable stiffness to investigate the influence of polymer flexibility on the dynamics of NPs of comparable size. The NPs exhibit subdiffusive dynamics on short time scales and diffusive dynamics on long time scales. With increasing polymer stiffness the long-time diffusivities of the NPs more markedly deviate from the SER, consistent with decoupling from the bulk polymer solution viscosity, and from PCT, which was developed for flexible polymers. The long-time diffusivities are adequately predicted by MCT, however, especially at high concentrations of the polymers where the theory is expected to be most accurate. On short time scales, the dynamics of the NPs become progressively more subdiffusive and decouple from the dynamics of the polymer chain center-of-mass as the stiffness of the polymer chains is increased. These changes in dynamics likely arise from differences in the segmental relaxations of the semiflexible chains. We anticipate that these predictions can be tested experimentally using, *e.g.*, nematic elastomers,[79,80] dendronized polymers,[81] or the well-characterized biopolymers ds-DNA or actin. Finally, the results from our computational study may aid in extending existing theories for describing NP transport in systems of flexible chains (*e.g.*, PCT) to solutions of stiff and semiflexible polymers.

Conflicts of interest

There are no conflicts to declare.

Acknowledgements

We thank Antonia Statt for sharing the implementation of RNEMD for MPCD in HOOMD-blue with us. This work was supported by the Welch Foundation (Grants E-1882 (J. C. P.) and E-1869 (J. C. C.)) and the National Science Foundation (CBET-1705968, to J. C. P. and J. C. C.). S. A. E. acknowledges financial support from the ACS-PRF grant No. 53934-ND6. A. N. received support from the German Research Foundation (DFG) under project number NI 1487/2-1. Computational resources were generously provided by the Center for Advanced Computing and Data Systems at the University of Houston.

References

1 K. S. Soppimath, T. M. Aminabhavi, A. R. Kulkarni and W. E. Rudzinski, *J. Controlled Release*, 2001, **70**, 1–20.
2 L. Tang, X. Yang, Q. Yin, K. Cai, H. Wang, I. Chaudhury, C. Yao, Q. Zhou, M. Kwon, J. A. Hartman, I. T. Dobrucki, L. W. Dobrucki, L. B. Borst, S. Lezmi, W. G. Helferich, A. L. Ferguson, T. M. Fan and J. Cheng, *Proc. Natl. Acad. Sci. U. S. A.*, 2014, **111**, 15344–15349.
3 E. Blanco, H. Shen and M. Ferrari, *Nat. Biotechnol.*, 2015, **33**, 941.

4 L. Satyanarayana, K. M. Reddy and S. V. Manorama, *Mater. Chem. Phys.*, 2003, **82**, 21–26.
5 J. S. Cooper, M. Myers, E. Chow, L. J. Hubble, J. M. Cairney, B. Pejcic, K.-H. Müller, L. Wieczorek and B. Raguse, *J. Nanopart. Res.*, 2014, **16**, 2173.
6 H. ShamsiJazeyi, C. A. Miller, M. S. Wong, J. M. Tour and R. Verduzco, *J. Appl. Polym. Sci.*, 2014, **131**, 40576.
7 G. Cheraghian and L. Hendraningrat, *Int. Nano Lett.*, 2016, **6**, 129–138.
8 B. Sarkar and P. Alexandridis, *Prog. Polym. Sci.*, 2015, **40**, 33–62.
9 Q. Chen, S. Gong, J. Moll, D. Zhao, S. K. Kumar and R. H. Colby, *ACS Macro Lett.*, 2015, **4**, 398–402.
10 T. G. Mason and D. A. Weitz, *Phys. Rev. Lett.*, 1995, **74**, 1250.
11 T. M. Squires and T. G. Mason, *Annu. Rev. Fluid Mech.*, 2010, **42**, 413–438.
12 M. E. Mackay, T. T. Dao, A. Tuteja, D. L. Ho, B. van Horn, H.-C. Kim and C. J. Hawker, *Nat. Mater.*, 2003, **2**, 762–766.
13 I. Y. Wong, M. L. Gardel, D. R. Reichman, E. R. Weeks, M. T. Valentine, A. R. Bausch and D. A. Weitz, *Phys. Rev. Lett.*, 2004, **92**, 178101.
14 A. Tuteja, M. E. Mackay, S. Narayanan, S. Asokan and M. S. Wong, *Nano Lett.*, 2007, **7**, 1276–1281.
15 R. A. Omari, A. M. Aneese, C. A. Grabowski and A. Mukhopadhyay, *J. Phys. Chem. B*, 2009, **113**, 8449–8452.
16 I. Kohli and A. Mukhopadhyay, *Macromolecules*, 2012, **45**, 6143–6149.
17 F. Babaye Khorasani, R. Poling-Skutvik, R. Krishnamoorti and J. C. Conrad, *Macromolecules*, 2014, **47**, 5328–5333.
18 R. Poling-Skutvik, R. Krishnamoorti and J. C. Conrad, *ACS Macro Lett.*, 2015, **4**, 1169–1173.
19 P. Nath, R. Mangal, F. Kohle, S. Choudhury, S. Narayanan, U. Wiesner and L. A. Archer, *Langmuir*, 2018, **34**, 241–249.
20 A. G. Ogston, B. N. Preston and J. D. Wells, *Proc. R. Soc. London, Ser. A*, 1973, **333**, 297–316.
21 L. Johansson, C. Elvingson and J. E. Loefroth, *Macromolecules*, 1991, **24**, 6024–6029.
22 R. I. Cukier, *Macromolecules*, 1984, **17**, 252–255.
23 A. R. Altenberger, M. Tirrell and J. S. Dahler, *J. Chem. Phys.*, 1986, **84**, 5122–5130.
24 G. D. J. Phillies, *Macromolecules*, 1986, **19**, 2367–2376.
25 H. Fujita, *Adv. Polym. Sci.*, 1961, **3**, 1–47.
26 S. A. Egorov, *J. Chem. Phys.*, 2011, **134**, 84903.
27 U. Yamamoto and K. S. Schweizer, *J. Chem. Phys.*, 2011, **135**, 224902.
28 U. Yamamoto and K. S. Schweizer, *Macromolecules*, 2015, **48**, 152–163.
29 L.-H. Cai, S. Panyukov and M. Rubinstein, *Macromolecules*, 2011, **44**, 7853–7863.
30 P.-G. de Gennes, *Scaling Concepts in Polymer Physics*, Cornell University Press, 1979.
31 F. Brochard Wyart and P. de Gennes, *Eur. Phys. J. E: Soft Matter Biol. Phys.*, 2000, **1**, 93–97.
32 R. Poling-Skutvik, K. I. S. Mongcopa, A. Faraone, S. Narayanan, J. C. Conrad and R. Krishnamoorti, *Macromolecules*, 2016, **49**, 6568–6577.
33 A. Chen, N. Zhao and Z. Hou, *Soft Matter*, 2017, **13**, 8625–8635.
34 R. Chen, R. Poling-Skutvik, A. Nikoubashman, M. P. Howard, J. C. Conrad and J. C. Palmer, *Macromolecules*, 2018, **51**, 1865–1872.
35 W. G. Miller, C. C. Wu, E. L. Wee, G. L. Santee, J. H. Rai and K. G. Goebel, *Pure Appl. Chem.*, 1974, **38**, 37–58.
36 M. Dijkstra and D. Frenkel, *Phys. Rev. E: Stat. Phys., Plasmas, Fluids, Relat. Interdiscip. Top.*, 1995, **51**, 5891.
37 S. A. Egorov, A. Milchev, P. Virnau and K. Binder, *Soft Matter*, 2016, **12**, 4944–4959.
38 X. Xu and J. Chen, *ACS Macro Lett.*, 2017, **6**, 331–336.
39 A. N. Semenov, *J. Chem. Soc., Faraday Trans. 2*, 1986, **82**, 317–329.
40 A. Nikoubashman, A. Milchev and K. Binder, *J. Chem. Phys.*, 2016, **145**, 234903.
41 A. Nikoubashman and M. P. Howard, *Macromolecules*, 2017, **50**, 8279–8289.
42 M. Otten, A. Nandi, D. Arcizet, M. Gorelashvili, B. Lindner and D. Heinrich, *Biophys. J.*, 2012, **102**, 758–767.
43 M. E. Grady, E. Parrish, M. A. Caporizzo, S. C. Seeger, R. J. Composto and D. M. Eckmann, *Soft Matter*, 2017, **13**, 1873–1880.
44 T. Gisler and D. Weitz, *Phys. Rev. Lett.*, 1999, **82**, 1606–1609.
45 T. G. Mason, T. Gisler, K. Kroy, E. Frey and D. A. Weitz, *J. Rheol.*, 2000, **44**, 917–927.
46 D. C. Morse, *Phys. Rev. E: Stat. Phys., Plasmas, Fluids, Relat. Interdiscip. Top.*, 1998, **58**, R1237–R1240.
47 F. Gittes and F. C. MacKintosh, *Phys. Rev. E: Stat. Phys., Plasmas, Fluids, Relat. Interdiscip. Top.*, 1998, **58**, R1241–R1244.
48 S. Plimpton, *J. Comput. Phys.*, 1995, **117**, 1–19.
49 K. Kremer and G. S. Grest, *J. Chem. Phys.*, 1990, **92**, 5057–5086.
50 J. D. Weeks, D. Chandler and H. C. Andersen, *J. Chem. Phys.*, 1971, **54**, 5237–5247.
51 M. Bishop, M. H. Kalos and H. L. Frisch, *J. Chem. Phys.*, 1979, **70**, 1299–1304.
52 R. Faller, A. Kolb and F. Müller-Plathe, *Phys. Chem. Chem. Phys.*, 1999, **1**, 2071–2076.
53 R. Faller, F. Müller-Plathe and A. Heuer, *Macromolecules*, 2000, **33**, 6602–6610.
54 R. Faller and F. Müller-Plathe, *Chem. Phys. Chem.*, 2001, **2**, 180–184.
55 W. Humphrey, A. Dalke and K. Schulten, *J. Mol. Graphics*, 1996, **14**, 33–38.
56 A. Malevanets and R. Kapral, *J. Chem. Phys.*, 1999, **110**, 8605–8613.
57 Y.-G. Tao, I. O. Götze and G. Gompper, *J. Chem. Phys.*, 2008, **128**, 144902.
58 G. Gompper, T. Ihle, D. M. Kroll and R. G. Winkler, *Advanced Computer Simulation Approaches for Soft Matter Sciences III*, Springer, 2009, pp. 1–87.
59 R. Kapral, *Adv. Chem. Phys.*, 2008, **140**, 89.
60 E. Allahyarov and G. Gompper, *Phys. Rev. E: Stat. Phys., Plasmas, Fluids, Relat. Interdiscip. Top.*, 2002, **66**, 36702.
61 H. Noguchi, N. Kikuchi and G. Gompper, *EPL*, 2007, **78**, 10005.

62 T. Ihle and D. M. Kroll, *Phys. Rev. E: Stat., Nonlinear, Soft Matter Phys.*, 2001, **63**, 020201.
63 C.-C. C. Huang, R. G. Winkler, G. Sutmann and G. Gompper, *Macromolecules*, 2010, **43**, 10107–10116.
64 D. S. Bolintineanu, G. S. Grest, J. B. Lechman, F. Pierce, S. J. Plimpton and P. R. Schunk, *Comput. Part. Mech.*, 2014, **1**, 321–356.
65 F. Müller-Plathe, *Phys. Rev. E: Stat. Phys., Plasmas, Fluids, Relat. Interdiscip. Top.*, 1999, **59**, 4894.
66 J. A. Anderson, C. D. Lorenz and A. Travesset, *J. Comput. Phys.*, 2008, **227**, 5342–5359.
67 J. Glaser, T. D. Nguyen, J. A. Anderson, P. Lui, F. Spiga, J. A. Millan, D. C. Morse and S. C. Glotzer, *Comput. Phys. Commun.*, 2015, **192**, 97–107.
68 M. P. Howard, J. A. Anderson, A. Nikoubashman, S. C. Glotzer and A. Z. Panagiotopoulos, *Comput. Phys. Commun.*, 2016, **203**, 45–52.
69 M. P. Howard, A. Z. Panagiotopoulos and A. Nikoubashman, *Comput. Phys. Commun.*, 2018, **230**, 10–20.
70 D. M. Meter and R. B. Bird, *AIChE J.*, 1964, **10**, 878.
71 A. Rao, *Rheology of Fluid, Semisolid, and Solid Foods*, Springer, US, 3rd edn, 2014.
72 M. Rubinstein and R. H. Colby, *Polymer Physics*, Oxford University Press, New York, 2003.
73 I.-C. Yeh and G. Hummer, *J. Phys. Chem. B*, 2004, **108**, 15873–15879.
74 V. Pryamitsyn and V. Ganesan, *Phys. Rev. Lett.*, 2008, **100**, 128302.
75 S. A. Egorov, *J. Chem. Phys.*, 2003, **119**, 4798–4810.
76 V. Sorichetti, V. Hugouvieux and W. Kob, *Macromolecules*, 2018, **51**, 5375–5391.
77 D. Richter, K. Binder, B. Ewen and B. Stuehn, *J. Phys. Chem.*, 1984, **88**, 6618–6633.
78 J. Sprakel, J. van der Gucht, M. A. Cohen Stuart and N. A. M. Besseling, *Phys. Rev. Lett.*, 2007, **99**, 208301.
79 P. Poulin, H. Stark, T. C. Lubensky and D. A. Weitz, *Science*, 1997, **275**, 1770–1773.
80 H. Finkelmann, E. Nishikawa, G. G. Pereira and M. Warner, *Phys. Rev. Lett.*, 2001, **87**, 015501.
81 S. Förster, I. Neubert, A. D. Schlüter and P. Lindner, *Macromolecules*, 1999, **32**, 4043–4049.

